Ultrafast demagnetization and its relation to microscopic momentum scattering dynamics in a Rashba ferromagnet

Svenja Vollmar, Kai Leckron, and Hans Christian Schneider ⓞ*
Physics Department and Research Center OPTIMAS, University of Kaiserslautern-Landau,
P. O. Box 3049, 67663 Kaiserslautern, Germany

We analyze theoretically the demagnetization dynamics in a ferromagnetic model system due to the interplay of Rashba-type spin-orbit coupling and electron-electron Coulomb scattering. We compute the k-resolved electronic reduced spin-density matrix, including precessional dynamics around internal spin-orbit and exchange fields as well as the electron-electron Coulomb scattering for densities and spin coherences. Based on a comparison with numerical solutions of the full Boltzmann scattering integrals, we establish that the k-resolved reduced spin-density matrix dynamics are well described using a simpler generalized relaxation-time ansatz for the reduced spin-density matrix. This ansatz allows one to relate the complicated scattering dynamics underlying the demagnetization dynamics to a physically meaningful momentum relaxation time τ. Our approach reproduces the behavior of the demagnetization time $\tau_{\mathrm{m}} \propto 1/\tau$ and $\tau_{\mathrm{m}} \propto \tau$ for the limits of short and long τ, respectively, and is also valid for the intermediate regime. The ansatz is not limited to the specific form of spin-orbit coupling considered here and provides a tool to include the correct demagnetization behavior in approaches that treat other contributions to the magnetization dynamics such as transport or magnon/phonon dynamics.

I. INTRODUCTION

The relaxation of electrically or optically induced electronic spin polarizations in semiconductors and simple metals has been studied for more than 50 years and has important connections to the spin-dependent dynamics of electrons in ferromagnets. Spin-relaxation dynamics in semiconductors have often been interpreted in terms of three different "classical" mechanisms: Elliott-Yafet (EY), Dyakonov-Perel (DP), and Bir-Aronov-Pikus, which were invented, respectively, for semiconductors with degenerate bands, for electronic bands with small spin splitting, and small-band-gap systems with electron-hole exchange interactions; see Refs. [1,2] for a general overview. The most widely applicable EY and DP mechanisms were based originally on a combination of spin-orbit coupling (SOC) with electron-impurity and electron-phonon scattering. In semiconductor spintronics it was realized about 20 years ago that electron-electron scattering, which arises from the *spin-independent* Coulomb interaction, can also contribute to spin relaxation, even though this interaction does not directly couple electrons to the lattice. More precisely, it leads to spin dephasing in the presence of a k-dependent spin-orbit-induced splitting between ↑ and ↓ states, which can be described in terms of a k-dependent internal effective magnetic field [3,4].

In ferromagnetic metals, a pronounced quenching of the magnetization, which is mainly related to d-band electrons, can be observed after excitation with an ultrashort optical pulse. While this is a more sizable effect than the relaxation of an induced spin polarization of a small density of excited electrons in semiconductor s- or p-like bands, the concept of Elliott-Yafet spin dynamics via electron-phonon scattering [5] was introduced early on as a mechanism to explain the reduction of spin angular momentum observed in the demagnetization process of ferromagnets [6].

The present paper is concerned with the characteristics of magnetization dynamics that are caused by a "spin-relaxation-like" approach to magnetization dynamics. Compared to semiconductors, ferromagnetic metals possess a more complicated ground state with correlated d-electron bands at the Fermi level, more complicated elementary excitations (magnons), and a different electron-phonon coupling (spin-lattice coupling). The mechanism of incoherent electronic dynamics [7,8] together with spin-orbit coupling considered in this paper thus competes with or complements other mechanisms, such as (1) coherent electronic dynamics [9] coupling of Fermi-level electrons to more tightly bound orbitals, (2) direct angular momentum transfer to phonons [10,11], and (3) magnon interactions [12,13], to name only a few. The dominant scattering mechanisms contributing to the incoherent electron dynamics arise from the interaction with phonons and other electrons. Electron-phonon scattering is often regarded as important because it can lead to electronic spin flips via coupling to the lattice [6], which fits into the picture of a three-temperature model as the spin-lattice coupling. Theoretical calculations indicate that the *spin-dependent* part of the electron-phonon interaction, in which the phonons directly change the electron spin, gives only a small contribution to electronic dynamics [14,15]. Instead, the main impact of electron-phonon scattering is the *spin-independent* contribution to its matrix element. The spin-independent electronic

*hc.schneider@rptu.de

momentum scattering processes *in combination* with electronic precessional spin dynamics around internal spin-orbit fields are mainly responsible for the change in electronic spin polarization [16]. Reference [16] discusses this microscopic picture of electron-spin to lattice coupling in some detail and shows that the lattice acts as the spin sink. If the electron-phonon scattering contributes to magnetization dynamics mainly because it acts as a momentum scattering channel for electrons, then the electron-electron scattering provides an additional momentum scattering channel that should be even more important for highly excited electrons because it can act on an even shorter timescale of 10 fs. The demagnetization dynamics corresponding to the latter mechanism have so far been investigated at the level of Fermi's golden rule rates for transitions between spin-mixed states due to the Coulomb interaction [7,8]. This approach can explain a sizable contribution to demagnetization, in particular, if a dynamical Stoner exchange splitting is included [8,17].

In this paper we investigate the electron-electron scattering contribution to the spin-dependent dynamics in a ferromagnetic model system using a similar approach as we have employed for electron-phonon scattering [16]. That is, we go beyond Fermi's golden rule rates for Coulomb scattering between electronic distributions in k space and include the *precessional dynamics* of coherences, i.e., the off-diagonal components of the spin-density matrix, around anisotropic effective spin-orbit fields. We apply this treatment of the spin-dependent electronic dynamics to a ferromagnetic Rashba model. We choose this generic spin-orbit coupling over a d-band structure because of its simplicity, which makes the numerical calculations feasible, as we can work with analytical expressions for the electronic spinor states. Such a Rashba model has been applied to a simple model of spin-orbit coupling in a thin ferromagnetic film; see, e.g., Ref. [18], but it has its limitations. For instance, even if the electron spectrum of surface states in metals is well described by the Rashba Hamiltonian, the spin dynamics may not be [19].

Using a screening parameter to control the strength of the electron-electron Coulomb scattering, we find that the influence of this scattering mechanism, including its effects on the precessional dynamics, can be captured well using an extended relaxation-time ansatz with a single effective momentum relaxation time τ for any given interaction strength. The ansatz and the effective relaxation time provide an arguably more general description of relaxation processes than what can be obtained microscopically from our simple model band structure. In terms of this relaxation time we can consistently describe a whole range of different demagnetization behaviors from a proportionality to τ^{-1} to the proportionality to τ, including the important intermediate regime, which, to the best of our knowledge, has not been mapped out in a ferromagnetic system yet. For semiconductors and nonmagnetic metals, similar scalings of the spin-relaxation rates/times have been found in their dependence of quasiparticle broadening [20,21] and doping concentrations [22].

II. THEORETICAL APPROACH

Our theoretical approach to determine the demagnetization dynamics and the quantities involved in the electronic

dynamics under the influence of internal spin-orbit fields and electron-electron scattering proceeds by first determining the single-particle energies and states of the Bloch electrons in our model band structure and then setting up and numerically solving the dynamical equations for the reduced electronic spin-density matrix, including electron-electron Coulomb scattering. We then introduce here a relaxation-time ansatz that can approximate the spin-conserving electron-electron Coulomb scattering well. The ansatz involves only a single relaxation time and introduces a time-dependent effective quasi-equilibrium spin-density matrix, to which the system evolves during demagnetization and remagnetization.

A. Hamiltonian and dynamical equation

The derivation of equations of motion (EOMs) for the electron-electron interaction is closely related to what we have presented in Refs. [23] and [16], but the general approach has been well established for semiconductor spintronics earlier [24]. Here we only give a short overview of the model system, which uses a two-dimensional k space and applies to two-dimensional electron gases and, in our case, to ferromagnetic thin films. The single-particle states and energies can be obtained in closed form from the system Hamiltonian,

$$\hat{H}(\mathbf{k}) = \hat{H}_{\mathrm{kin}}(k) + \hat{H}_{\mathrm{SO}}(\mathbf{k}) + \hat{H}_{\mathrm{Stoner}}, \qquad (1)$$

with the effective-mass contribution $\hat{H}_{\mathrm{kin}}(k) = \frac{\hbar^2 k^2}{2m^*}$. The spin-orbit contribution is of the Rashba form and can be written in terms of the vector of Pauli matrices $\hat{\boldsymbol{\sigma}}$:

$$\hat{H}_{\mathrm{SO}}(\mathbf{k}) = \alpha(\hat{\boldsymbol{\sigma}} \times \mathbf{k}) \cdot \mathbf{e}_z = \alpha(\hat{\sigma}_x k_y - \hat{\sigma}_y k_x). \qquad (2)$$

The strength of the spin-orbit contribution to our effectively two-dimensional electron system is controlled by the Bychkov-Rashba parameter α. The mean-field Hubbard contribution leads to a Stoner contribution $\hat{H}_{\mathrm{Stoner}} = Um$, which depends on an effective on-site interaction energy U and the magnetization m. In the Stoner approach, the magnetization is essentially equal to the spin polarization. This quantity is defined in Eq. (7). We self-consistently determine the band structure and states *in equilibrium*, which results in an equilibrium spin polarization of $m \approx 0.454$ (0.5 would be the maximum spin polarization). We keep the band structure fixed throughout the dynamics, i.e., we do not self-consistently adjust the band structure to the instantaneous value of m, see also the discussion below.

Figure 1 illustrates the important features of the model. The model band structure exhibits a k-dependent band splitting and $\mathbf{k}$-dependent Bloch spinors, which we denote by $\Uparrow$ and $\Downarrow$ to indicate that they are not pure spin states. The splitting $\Delta E_k \equiv \varepsilon_{k\Uparrow} - \varepsilon_{k\Downarrow}$ of the bands shown in Fig. 1(a) ranges from $\Delta E_{k=0} = 400\,\mathrm{meV}$ to $\Delta E_{k=10\,\mathrm{nm}^{-1}} = 725\,\mathrm{meV}$ for different k values. Figures 1(b) and 1(c) depict the k-local spin expectation values $\langle \mathbf{k}\mu | \boldsymbol{\sigma} | \mathbf{k}\mu \rangle / 2$ for the Bloch spinors $|\mathbf{k}\mu\rangle$: (b) the longitudinal component vs k and (c) the components perpendicular to z vs polar angle for a fixed k. Around $k = 0$ states are essentially $\uparrow$ and $\downarrow$ spin states, but the mixing increases with increasing k, or equivalently, energy. For highly
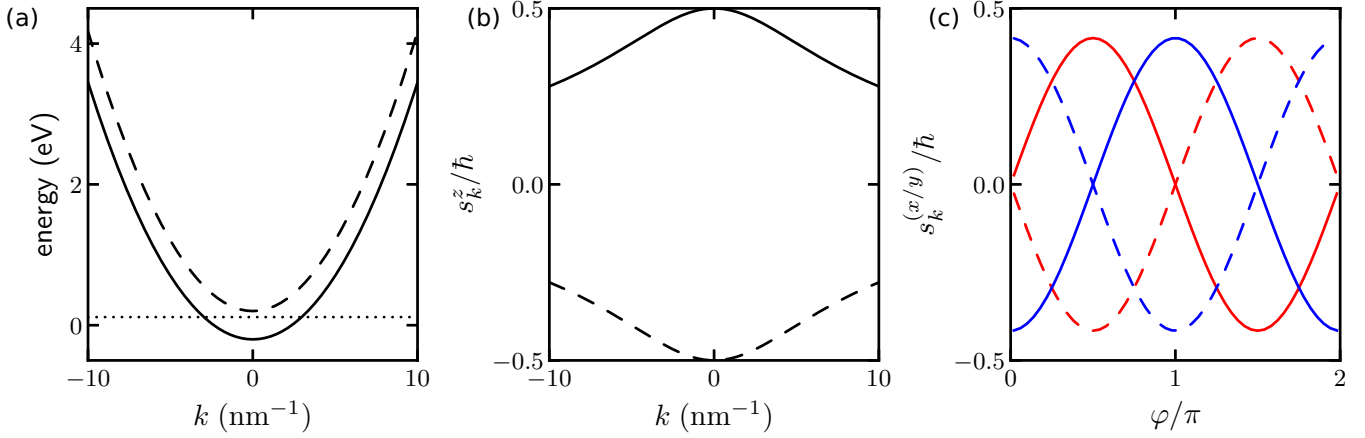
FIG. 1. Self-consistently calculated k-dependent band structure (a) with the corresponding spin structure in z direction (b). The φ-dependent spin structure in x (red) and y (blue) direction are shown for a fixed $k = 10$ nm^{-1} (c). The solid lines correspond to the energies and k-local quantization axes in the lower band, the dashed lines to those in the upper band. The parameters used throughout this paper are Stoner interaction parameter $U = 400$ meV, Rashba parameter $\alpha = 30$ meV nm, electron density $n_e = 0.7$ nm^{-1}. At each k point, the quantization axis of the upper and lower bands point in opposite directions.

excited electrons at k states as shown in Fig. 1(c), the Bloch states are considerably spin mixed. The parameters given in Fig. 1 and throughout this paper are chosen to mimic a strong ferromagnet. The strength of the Rashba parameter is chosen considerably larger than in the prototypical GaAs-based semiconductors, where mainly s electrons contribute, but smaller than in a system with "giant-Rashba" splitting [25].

The electronic quantum state is described by the reduced spin-density matrix $\rho_{\mathbf{k}}^{\mu\mu'} = \langle \hat{c}_{\mathbf{k}\mu}^{\dagger} \hat{c}_{\mathbf{k}\mu'} \rangle$, where $\hat{c}_{\mathbf{k}\mu}^{(\dagger)}$ is the annihilation (creation) operator of an electron with momentum $\mathbf{k}$ in band μ. In the EOM for the spin-density matrix, we include the electron-electron Coulomb interaction at the level of second Born scattering integrals, which can be derived using Green's function or reduced density-matrix techniques [26–28]:

$$\frac{\partial}{\partial t}\rho_{\mathbf{k}}^{\mu\mu'} = \frac{i}{\hbar}(\varepsilon_{\mathbf{k}\mu} - \varepsilon_{\mathbf{k}\mu'})\rho_{\mathbf{k}}^{\mu\mu'} + \frac{\pi}{\hbar}\sum_{\mathbf{lq}}\sum_{\substack{\mu_1\mu_2\mu_3\\\mu_4\mu_5\mu_6\mu_7}}\left(V_{\mathbf{klq}}^{\mu\mu_1\mu_2\mu_3}\right)^*\left(V_{\mathbf{klq}}^{\mu_4\mu_5\mu_6\mu_7} - V_{\mathbf{l+qlk-l}}^{\mu_4\mu_5\mu_6\mu_7}\right)\delta\left(\Delta E_{\mathbf{klq}}^{\mu_4\mu_5\mu_6\mu_7}\right)$$

$$\times \left[\rho_{\mathbf{k+q}}^{\mu_3\mu_7}\rho_{\mathbf{l}}^{\mu_2\mu_6}\left(\delta_{\mu_1\mu_5}-\rho_{\mathbf{l+q}}^{\mu_5\mu_1}\right)\left(\delta_{\mu'\mu_4}-\rho_{\mathbf{k}}^{\mu_4\mu'}\right)-\rho_{\mathbf{k}}^{\mu_4\mu'}\rho_{\mathbf{l+q}}^{\mu_5\mu_1}\left(\delta_{\mu_2\mu_6}-\rho_{\mathbf{l}}^{\mu_2\mu_6}\right)\left(\delta_{\mu_3\mu_7}-\rho_{\mathbf{k+q}}^{\mu_3\mu_7}\right)\right]$$

$$+ \frac{\pi}{\hbar}\sum_{\mathbf{lq}}\sum_{\substack{\mu_1\mu_2\mu_3\\\mu_4\mu_5\mu_6\mu_7}}V_{\mathbf{klq}}^{\mu'\mu_1\mu_2\mu_3}\left(V_{\mathbf{klq}}^{\mu_4\mu_5\mu_6\mu_7} - V_{\mathbf{l+qlk-l}}^{\mu_4\mu_5\mu_6\mu_7}\right)^*\delta\left(\Delta E_{\mathbf{klq}}^{\mu_4\mu_5\mu_6\mu_7}\right)$$

$$\times \left[\rho_{\mathbf{k+q}}^{\mu_7\mu_3}\rho_{\mathbf{l}}^{\mu_6\mu_2}\left(\delta_{\mu_5\mu_1}-\rho_{\mathbf{l+q}}^{\mu_1\mu_5}\right)\left(\delta_{\mu_4\mu}-\rho_{\mathbf{k}}^{\mu\mu_4}\right)-\rho_{\mathbf{k}}^{\mu\mu_4}\rho_{\mathbf{l+q}}^{\mu_1\mu_5}\left(\delta_{\mu_6\mu_2}-\rho_{\mathbf{l}}^{\mu_6\mu_2}\right)\left(\delta_{\mu_7\mu_3}-\rho_{\mathbf{k+q}}^{\mu_7\mu_3}\right)\right]. \tag{3}$$

The first row describes a coherent precession of the off-diagonal contributions of the spin-density matrix, i.e., the *coherences* $\rho_{\mathbf{k}}^{\mu\mu'}$, $\mu \neq \mu'$, due to the splitting between the bands μ and μ' at $\mathbf{k}$. The remaining terms are electron-electron scattering contributions with the Coulomb-matrix elements $V_{\mathbf{klq}}^{\mu_1\mu_2\mu_3\mu_4} \equiv V_{\mathbf{k,l+q\rightarrow k+q,l}}^{\mu_1\mu_2\mu_3\mu_4} = V_q\langle \mathbf{k}\mu_1|\mathbf{k}+\mathbf{q}\mu_4\rangle\langle \mathbf{l}+\mathbf{q}\mu_2|\mathbf{l}\mu_3\rangle$, where V_q denotes a *screened* Coulomb potential depending on the momentum $\mathbf{q}$ transferred from the electron with initial momentum $\mathbf{k}$ to the electron with final momentum $\mathbf{l}$, i.e., $\mathbf{k} \rightarrow \mathbf{k}+\mathbf{q}$ and $\mathbf{l}+\mathbf{q} \rightarrow \mathbf{l}$ and with the argument of the energy difference $\Delta E_{\mathbf{klq}}^{\mu_4\mu_5\mu_6\mu_7} = \varepsilon_{\mathbf{k}\mu_5} + \varepsilon_{\mathbf{l+q}\mu_6} - \varepsilon_{\mathbf{l}\mu_6}\varepsilon_{\mathbf{k+q}\mu_7}$, which as an argument of a δ function guarantees energy conservation. To obtain the Boltzmann-like scattering integrals in Eq. (3) one has to employ a Markov approximation not only for real occupation-number distributions but also for complex coherences with a precessional

contribution stemming from the first term. This precessional frequency is removed by transforming to a rotating frame, in which the Markov approximation can be made, and then transforming back [24,29,30]. A physical interpretation of lines 2–5 in Eq. (3) lies in Fermi's golden rule, which yields scattering rates for Fermionic occupation numbers/probabilities of initial and final states $n\,n\,(1-n)\,(1-n)$, as sketched in Fig. 2. The many-particle approach used here extends these quantities to the off-diagonal elements of the spin-density matrix., i.e., coherences between different spin states.

Since the $\mathbf{k}$ space for the single-particle states defined above is two dimensional (2D), we use the screened Coulomb potential in two dimensions in the form $V_q = \frac{e^2}{2\mathcal{V}\varepsilon_0\varepsilon_b(q+\kappa)}$ [31] with the elementary charge e, the normalization volume $\mathcal{V}$, the dielectric constant ε_0, the screening constant ε_b, and the screening parameter κ. Below we analyze the dependence of
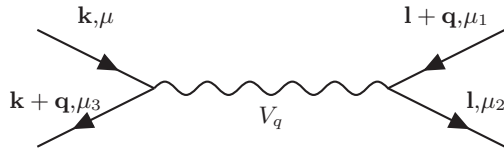
FIG. 2. Sketch of the two-electron scattering process mediated by the Coulomb interaction as it applies to a scattering process between electronic distributions for incoming electronic states $(\mathbf{k}, \mu)$, $(\mathbf{l} + \mathbf{q}, \mu_1)$ and outgoing electronic states $(\mathbf{k} + \mathbf{q}, \mu_3)$, $(\mathbf{l}, \mu_2)$ with up and/or down spins defined with respect to the k-dependent local quantization axis. The influence of scattering on the coherences involves additional band indices that describe the noncollinear electron spins.

the dynamics in dependence of the inverse screening length, which is determined by the band structure, carrier density, and possibly by the dielectric environment. In our simplified band structure we essentially regard this as a model parameter and choose values on the order of 20 nm^{-1} and smaller. This value is consistent with a calculation of the screening parameter κ for electrons in parabolic bands [26,31] in the 2D limit via $\kappa = m^* e^2 / (2\pi \hbar^2 \varepsilon_b \varepsilon_0) f(k = 0)$ with a relative background screening constant of $\varepsilon_b = 1$.

One goal of this paper is to compare and contrast the electronic dynamics described by the full density matrix with those obtained using *occupation numbers*. In principle, an approach that uses only occupation numbers $n_{\mathbf{k}}^{\mu} := \rho_{\mathbf{k}}^{\mu\mu}$, i.e., the diagonal elements of the density matrix, is an approximation to the full density matrix. In this case, the Boltzmann scattering integrals are essentially rates as one would obtain from Fermi's golden rule, which connect nonpure spin states and thus lead to spin-flip transitions [6,32]. Because the Coulomb interaction is spin independent, the Coulomb scattering *alone* cannot cause a transition that changes the magnetization. For electron scattering dynamics between nonpure spin states, the restriction to occupation dynamics, which neglects the influence of the off-diagonal parts of the spin-density matrix, means that there is no conservation of ensemble spin, and one obtains demagnetization due to Coulomb scattering [7,8]. In order to elucidate this, we also evaluate Eq. (3) at the level of Fermi's golden rule for occupations. This approach is often called "Boltzmann scattering," but this may cause confusion in our case because we also have Boltzmann-like scattering integrals for *all* elements of the spin-density matrix in the complete EOM (3). To differentiate between the full spin-density matrix calculation and the calculation that uses only the occupations, we refer to them as "generalized Boltzmann scattering" (or simply "full") and "occupation-number approximation", respectively.

B. Relaxation-time approximation

In addition to the dynamics of the spin-density matrix with generalized Boltzmann scattering, which is nonlocal in k space, we will use a relaxation-time ansatz that is designed specifically for spin-polarized systems with spin-orbit coupling. In Ref. [33] we applied the ansatz in the context of optically driven dynamics. We stress that it allows one to replace the complexity of the scattering integrals by introducing

a single physically meaningful relaxation time that characterizes the complex, k-dependent scattering dynamics. It thus provides a simple and intuitive but also accurate description of this scattering process that should also have applications to calculations involving transport and/or in combination with other scattering mechanisms, such as electron-magnon scattering.

The ansatz is based on suitably defined quasi-equilibrium density matrices of the general form

$$\tilde{\rho}_{\text{eq}} = f(T, \mu, \zeta_z), \tag{4}$$

where f is a Fermi-Dirac distribution depending on temperature T, chemical potential μ, and spin accumulation ζ. The parameters T, μ, and ζ are determined such that the distribution reproduces a prescribed charge density, energy density, and spin polarization. In this work we only consider the spin polarization in z direction due to the symmetries of our model system. The grand-canonical Hamiltonian for noninteracting electrons corresponding to Eq. (4) is

$$\hat{K} = \hat{H} + \mu \hat{N} - \zeta_z \hat{\sigma}_z, \tag{5}$$

where $\hat{H}$ is the many-particle Hamiltonian corresponding to (1) discussed above, and $\hat{N}$ is the particle number operator.

The expectation values of the particle density, the spin polarization, and the energy density used in the quasi-equilibrium distribution (4) will be obtained from those of the nonequilibrium density matrix ρ as it arises during the dynamics and are calculated as follows. The electron density is given by

$$n_{\text{e}} = \frac{1}{\mathcal{V}} \sum_{\mu} \sum_{\mathbf{k}} \rho_{\mathbf{k}}^{\mu\mu}, \tag{6}$$

the spin polarization/magnetization m by

$$m = \frac{1}{\mathcal{V} n_{\text{e}}} \sum_{\mu\mu'} \sum_{\mathbf{k}} \langle \mathbf{k}\mu | \hat{s}_z | \mathbf{k}\mu' \rangle \rho_{\mathbf{k}}^{\mu\mu'}, \tag{7}$$

and the energy density ε by

$$\varepsilon = \frac{1}{\mathcal{V}} \sum_{\mu} \sum_{\mathbf{k}} \varepsilon_{\mathbf{k}\mu} \rho_k^{\mu\mu'}. \tag{8}$$

Here $\mathcal{V}$ is the normalization volume. Note, in particular, that the spin-polarization dynamics also include the microscopic coherences $\rho_{\mathbf{k}}^{\mu\mu'}$, $\mu \neq \mu'$, and that, since we will only be discussing the relative change of the spin polarization further below, *magnetization* and *spin polarization* are interchangeable.

Our relaxation-time approximation consists of replacing the scattering integrals by the following contribution to the equation of motion for the spin-density matrix:

$$\frac{\partial}{\partial t} \rho_{\mathbf{k}}^{\mu\mu'} \bigg|_{\text{rel}} = -\frac{\rho_{\mathbf{k}}^{\mu\mu'} - \tilde{\rho}_{\mathbf{k}}^{\mu\mu'}}{\tau}. \tag{9}$$

Here $\tilde{\rho}_{\mathbf{k}}^{\mu\mu'}$ is the *quasi-equilibrium* reduced spin-density matrix introduced in Eq. (4), which is diagonal in the eigenbasis of the grand-canonical single-particle Hamiltonian $\hat{K}$, see Eq. (5). The dynamics of the spin-density matrix $\rho_{\mathbf{k}}^{\mu\mu'}$, however, are calculated in the eigenbasis of the regular single-particle Hamiltonian so that one must transform the density

matrix accordingly, i.e., from the eigenbasis of $\hat{K}$ to that of $\hat{H}$. Due to the transformation between the $\hat{K}$ and $\hat{H}$ bases, $\tilde{\rho}_{\mathbf{k}}^{\mu\mu'}$, which is diagonal in the grand-canonical basis, has off-diagonal elements in the basis of $\hat{H}$ and therefore also describes the influence of scattering processes on the off-diagonal elements of the spin-density matrix, which are needed for the correct determination of the ensemble spin expectation value, i.e., the magnetization. With this approach our Eq. (9) employs only a single relaxation time τ and mimics incoherent electron-electron scattering as it conserves the respective conservation laws. Note that the relaxation time is by construction independent of k and energy and acts in a different way compared to relaxation times that are usually introduced as energy-dependent out-scattering rates and then averaged over suitably chosen quasi-equilibrium distribution functions [34,35]. Such an ansatz can also model spin-conserving electron-phonon scattering if one uses a different quasi-equilibrium distribution with a fixed temperature of the phonon bath T_{pn}. In this case, one only needs to determine μ and ζ in order to conserve density and spin polarization.

C. Model parameters and initial conditions

The magnetization dynamics discussed below start from a magnetic equilibrium state, and since the Stoner contribution of the Hamiltonian (1) depends on the spin polarization m of the system, this equilibrium state is determined self-consistently (see Sec. II D below for more details).

In order to achieve a comparison of the different magnetization dynamics, we employ a simple model excitation by an ultrashort optical pulse. As before [16,36], we assume that the electronic energy is instantaneously raised to an excitation temperature $T_{\mathrm{ex}} \gg T_{\mathrm{eq}} = 100$ K and the excited electrons are distributed according to Eq. (10) with the excitation temperature in the self-consistently determined band structure. We stress that, as mentioned above, we keep the band structure fixed throughout the dynamics. A reduction of the band gap usually has little impact on the demagnetization time constant, resulting mainly in a more pronounced demagnetization [8,17]. Hence, we use a constant gap, as this also helps to reduce the numerical complexity. In the following we vary the interaction strength via the screening parameter κ. The Rashba parameter α is kept fixed because it would not only change the interaction strength (via the matrix elements) but also the band structure features and the equilibrium magnetization.

The instantaneous heating leads to different chemical potentials for the $\Uparrow$ and $\Downarrow$ bands, as well as to a small change of the spin polarization m due to the $\mathbf{k}$-dependent spin mixing of the states. This approach does not change the electronic density in each band and is numerically simple and controllable by a single parameter T_{ex}; it is designed to capture qualitatively the effect of an ultrashort pulse that deposits energy in the electronic system; see, e.g., Ref. [14] for a more detailed description of this process. With this model of the excitation process we neglect optically driven interband coherences that may be excited by the excitation pulse, as the purpose of this paper is to analyze the possible dynamics in the incoherent regime.

We choose an excitation temperature T_{ex} of 4000 K in order to clearly exhibit the dynamical features. This quantity characterizes an electronic excited state far from equilibrium and should therefore not be compared to an equilibrium quantity, such as the Curie temperature, which is $T_{\mathrm{C}} \approx 1030$ K for the model parameters listed in Fig. 1.

D. Numerical considerations

Restricting the model to two dimensions greatly simplifies the numerical calculations, in particular, the summations over momenta $\mathbf{k}$, $\mathbf{l}$, and $\mathbf{q}$ on the right-hand side of Eq. (3), which have to be calculated in every time step. Even in 2D, the numerical solution of the EOM (3) requires a considerable accuracy to keep the numerical errors from accumulating over the demagnetization and remagnetization dynamics, which would spoil the important conservation laws. We thus use a Runge-Kutta-type integration method developed by Dormand and Prince [37], with a dynamical time-step control to keep a high accuracy while also optimizing the CPU time.

The relaxation-time approximation introduced above has a much lower numerical cost and better scaling, due to the lack of nested summations over momenta k(l)(q) as they occur in the time integration of Eq. (3). It is anticipated that this enormous advantage in computational time and effort will allow an application in three-dimensional multiband structures in the future.

The initial equilibrium state is calculated as follows: We start from an arbitrary value of m in z direction to set the preferential direction and iteratively (i) calculate the new band structure according to m, (ii) populate this band structure with electronic equilibrium (Fermi) distributions

$$\rho_k^{\mu\mu'} = \frac{1}{e^{\beta(\varepsilon_{k\mu}-\mu_{\mathrm{C}})}+1}\delta_{\mu\mu'}, \tag{10}$$

by adjusting the chemical potential μ_{C} such that our desired electronic density n_{e} for a given equilibrium temperature T_{eq} is reproduced, and (iii) calculate the new spin polarization m_{new} in this band structure and repeat steps (i)–(iii) until the spin-polarization difference Δm between two consecutive iterations is small enough (we chose $\Delta m < 10^{-9}$).

III. RESULTS

We start with the generalized Boltzmann scattering. The main quantity of interest to us is the time dependence of the magnetization m, i.e., the spin polarization of the electrons in the split bands. As it is our goal to compare the dynamics for different ratios of typical scattering times to typical precession times, we choose here to vary *only* the screening parameter κ, which changes the matrix element of the Coulomb interaction and thus the k-dependent scattering rates. Using this one adjustable parameter to control the Coulomb scattering rates, we intend to illustrate the range of possible behaviors of the magnetization dynamics and how well these can be captured with our extended relaxation-time ansatz. We therefore make no effort here to connect κ to a variable that can be tuned in experiment.

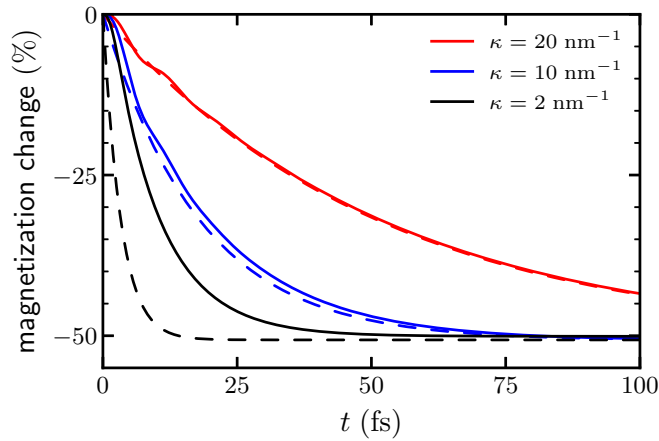Figure 3 shows the demagnetization dynamics obtained for the excitation conditions discussed in Sec. II C. Shown

FIG. 3. Relative magnetization change vs time for different screening parameters κ for the full calculation (solid lines) and the occupation-number approximation (dashed lines).

FIG. 4. Same data as in Fig. 3 displayed with a logarithmic time axis to emphasize the short-time dynamics. Regardless of κ, there is only a marginal magnetization change for the full calculation (solid lines) on short times <4 fs, since the buildup of the coherences is limited by the precession time of ≈ 10 fs. The demagnetization process in the occupation-number approximation starts at arbitrarily early times for stronger scattering, i.e., smaller κ.

are the relative magnetization changes resulting from the full calculation (solid lines) and using the occupation-number approximation (dashed lines) for small, intermediate, and large screening parameters $\kappa = 2$ nm^{-1}, $\kappa = 10$ nm^{-1}, and $\kappa = 20$ nm^{-1}. We do not include electron-phonon coupling, or any other coupling, to an energy bath that would absorb the energy transferred to the electronic system by the optical excitation over time. The system therefore stays in a partially demagnetized state even for times $t \gtrsim 0.1$ ps. As described in the last section, we do not include a dynamical band structure, which would lead to a more pronounced demagnetization, likely close to a complete demagnetization for our very strong excitation conditions.

For the occupation-number approximation a smaller screening parameter κ (faster scattering) always leads to faster spin/magnetization dynamics. In the full calculation this behavior is also visible but less pronounced, and the magnetization dynamics only coincide for larger κ (slower scattering) with those of the occupation-number approximation. For values of $\kappa \lesssim 5$ nm^{-1} the two calculations deviate at shorter times and the demagnetization dynamics of the full calculation are considerably slower. This is shown more prominently in Fig. 4, which plots the same curves vs a logarithmic time scale to display the behavior at very short timescales. Around and below the precession time $T_\mathrm{p} = h/\Delta E_k \approx 10$ fs one observes that T_p effectively sets a lower limit for any magnetization change by this mechanism. The reason for this discrepancy is that the occupation-number dynamics neither include precessional spin dynamics nor its dephasing due to the Coulomb interaction. The Golden-Rule-like scattering in the occupation-number dynamics simply gets faster for larger interaction matrix elements.

In an earlier paper [16] we have studied the influence on spin dephasing of electron-longitudinal-phonon scattering, for which the typical momentum scattering times are longer than the precession times of electronic spins around typical exchange fields (determined by the exchange splitting between the bands). For this mismatch of scattering and precession times, we found that the occupation-number approximation agreed well with the full calculation, and that it is thus justified
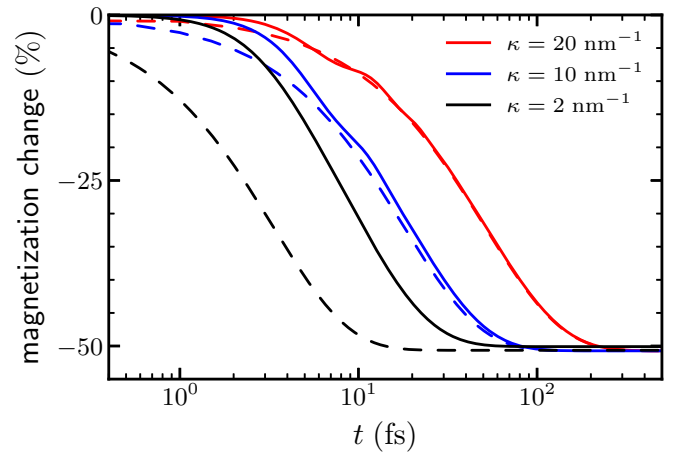
to use an Elliott-Yafet like description, i.e., an incoherent scattering process that leads to a spin change, or, as it is often called, a spin flip, and exhibits a linear time-dependence of demagnetization times on typical electron-phonon scattering times. For the electron-electron scattering considered in this paper, the occupation-number approximation reproduces the result of the full calculation *only* for stronger screening effects. The discrepancy between the occupation-number approximation and the full dynamics should be even more pronounced in systems with a smaller splitting, where the precession frequencies are smaller.

In Fig. 5 we turn to a comparison of the full calculation with the relaxation-time ansatz. We start with the demagnetization characteristics as obtained for two different screening parameters and suitably chosen relaxation times τ
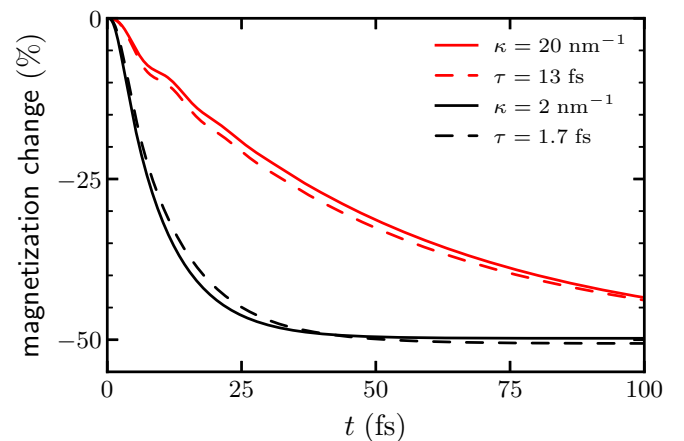

FIG. 5. Relative magnetization change vs time for the full calculation with two different screening parameters (solid lines) and two relaxation-time calculations (dashed lines). The remaining parameters are as in Fig. 3.

FIG. 6. Real (top) and imaginary part (bottom) of the coherence at a k-point $\tilde{k} = 3.3$ nm^{-1} near the Fermi edge vs time for the full calculation with two different screening parameters (solid lines) and two relaxation-time calculations (dashed lines). The remaining parameters are as in Fig. 3.
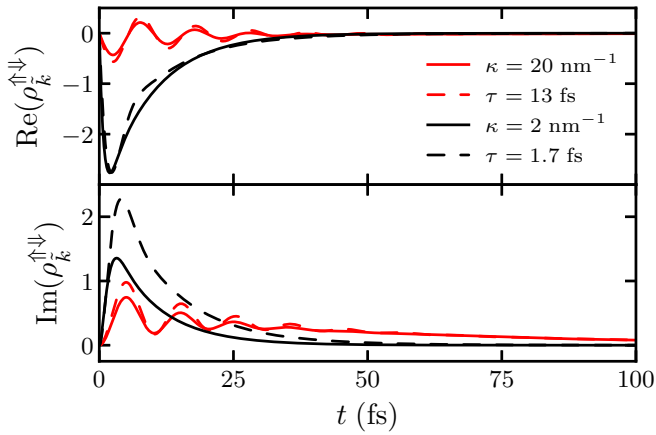

FIG. 7. Demagnetization time vs effective scattering time τ with a fit. The remaining parameters are as in Fig. 3.

for each screening parameter. We obtain a good agreement of the demagnetization dynamics between the $\kappa = 20$ nm^{-1} and $\tau = 13$ fs curves, as well as between the $\kappa = 2$ nm^{-1} and $\tau = 1.7$ fs curves. This is already a satisfying result, as a look back to Fig. 3 shows that such a good agreement for different κ values cannot be achieved using the occupation-number approximation. However, the magnetization change is a k-integrated quantity, and we would also like to compare the k-resolved dynamics.

Figure 6 compares the results of the full calculation and the relaxation-time approximation for the dynamics of the coherence $\rho_k^{\Uparrow\Downarrow}$ at $\tilde{k} = 3.3$ nm^{-1} for different values of κ. This particular $\tilde{k}$ is located near the Fermi edge of the lower band so that its dynamics play an important role during the whole demagnetization process. The different k resolved dynamics for the two cases that arise in the full microscopic calculation are reproduced well by the calculation with the extended relaxation-time ansatz. For the full calculation and the relaxation-time ansatz, precessional dynamics of the coherence are clearly visible at early times $t \lesssim 30$ fs for $\kappa = 20$ nm^{-1} and the fit with $\tau = 13$ fs. There are two contributions we want to discuss here. First, the precessional dynamics are driven by scattering events $\mathbf{k} \rightarrow \mathbf{k} + \mathbf{q}$ which conserve the vector spin and thus lead to a mismatch of the spin with the local quantization axis at $\mathbf{k} + \mathbf{q}$. Second, the scattering also dephases the precession of the spin coherences toward a finite value at around $t = 30$ fs, at which time the demagnetization is not even half completed (see Fig. 3). After that time there is only a slow relaxation of the spin coherence. This result is qualitatively similar to that obtained for spin-conserving electron-phonon scattering [16].

For $\kappa = 2$ nm^{-1} in the full calculation, the respective $\tau = 1.7$ fs that fits best in the relaxation-time approach becomes shorter by a factor of 8, indicating a much faster scattering. In this case one cannot discern a precessional motion in the coherence but rather strongly damped dynamics with one intermittent maximum. The whole spin-density dynamics here occurs on essentially the same timescale as the corresponding
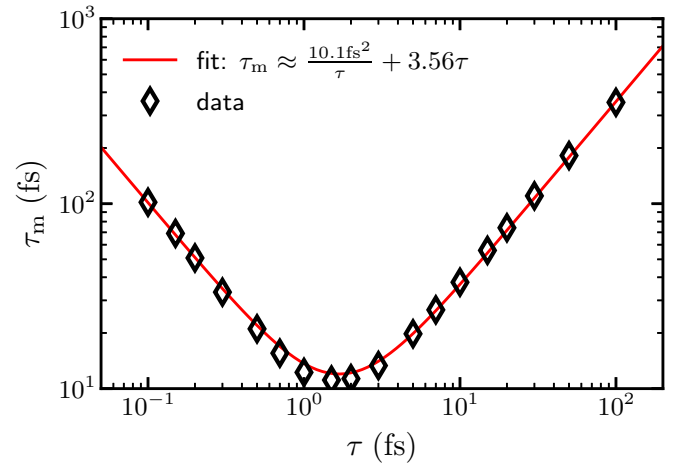
demagnetization curve in Fig. 5. In both cases the relaxation-time ansatz comes close to the full calculation, even though it replaces the complicated electron-electron scattering dynamics in k space by a k-local expression with a constant, i.e., k-independent, relaxation time. That the quantitative agreement of the k-resolved and k-integrated quantities is so good is likely also due to our model excitation, which creates excited electron distributions that are close to hot Fermi-Dirac distributions. For excitations that exhibit stronger nonequilibrium characteristics, the quantitative agreement may not be quite as good, but the relaxation-time approximation should still capture the most important features of the spin-dependent electronic scattering dynamics.

Up to now we have demonstrated that the relaxation-time ansatz reproduces the magnetization dynamics due to precessional dynamics and scattering quite well. Because the complicated scattering dynamics are parametrized by the relaxation time τ, we can use it to study the influence of scattering on the electronic spin-dependent dynamics via this single parameter. For a range of relaxation times τ, we calculate the demagnetization curves as in Fig. 5 and subsequently extract the *demagnetization time* τ_{m} by fitting the demagnetization dynamics by an exponential function $m(t) = b - a \exp(-t/\tau_{\mathrm{m}})$. Figure 7 plots the demagnetization times obtained from this fitting procedure vs the relaxation time τ as black diamonds. For long relaxation times τ, the demagnetization time increases with τ, but for short relaxation times, it increases with *decreasing* τ. The scaling for small and large τ is in agreement with that found in Ref. [22] for electronic dynamics in quantum wells. Importantly, there exists a minimum of $\tau_{\mathrm{m}}(\tau)$ for intermediate τ. Calculations using the occupation-number approximation (not shown) miss the behavior at small τ and yield only a steady decrease of τ_{m} with decreasing relaxation times τ. This behavior is already evident in Fig. 3 where the occupation-number approximation leads to ever faster demagnetization.

The quantitative dependence of τ_{m} on τ is fit to the following expression:

$$\tau_{\mathrm{m}} = \frac{A}{\tau} + B\tau. \tag{11}$$

This simple parametrization of the relaxation time contains as limits the simple forms of the Dyakonov-Perel mechanism for small and large τ, which are well known in spintronics [2]. The result is shown as red solid line in Fig. 7. We see a remarkably good agreement of the fit and the extracted demagnetization times from the relaxation-time calculations. The parameter $A = 10.1$ fs^2 can be put into correspondence with the precession frequency of the spin-splitting $\hbar\Omega = \Delta E_k$ via $A \simeq \Omega^{-2}$. In the short τ limit we thus obtain a connection $\tau_m \approx \Omega^{-2}/\tau$. The form of Eq. (11) has already been suggested by Refs. [20,21]. It can be obtained, for instance, from a thermal Green function approach to spin relaxation in semiconductors and metals. The relation of the spin-relaxation time to a characteristic time $\tau_0 = \gamma^{-1}$ in Refs. [20,21] is very similar to ours, but there the momentum scattering rates are related to lifetimes at the Fermi energy. Our results suggest that the scaling of the demagnetization time with τ is rather robust and also valid for excited systems with electronic populations far away from the Fermi energy if τ is interpreted as in Eqs. (4) and (9).

While the behavior for short τ is reminiscent of typical spin-dephasing mechanisms of spintronics, the same microscopic interplay of precessional spin dynamics around internal fields with a spin-independent scattering mechanism is behind the demagnetization dynamics *for the whole range* of τ shown in Fig. 7. In particular, for larger τ we obtain the inverse relation $\tau_m \propto \tau$. Such a relation is usually associated with spin relaxation, as it occurs via spin-flip transitions due to an explicitly spin-dependent interaction. Figure 7 shows clearly that both behaviors occur as limiting cases for small and large τ, respectively, for electrons in a ferromagnetic band structure with spin-orbit coupling. For intermediate τ of about 1–10 fs a minimum of demagnetization times occurs, which is also very well described by the fit curve. The range around the minimum is likely close to the realistic range for metallic systems. We believe that the result contained in Fig. 7 gives an accurate and intuitive picture of electron-electron scattering dynamics in highly excited ferromagnets by identifying τ as a physically meaningful parameter. One can thus use it as a fit parameter also for systems that are not described by the model band structure used in this paper. This makes it possible to extract τ from measured τ_m data via a fit, or obtain $\tau_m(\tau)$ from numerical calculations solving the full Boltzmann scattering problem. Figure 7 is particularly important for fits to experimental τ_m data. If one does not include the nonlinear regime at small τ and assumes a linear relation between τ_m

and τ, one would greatly overestimate the actual momentum relaxation time and miss the contribution from the precessional dynamics completely. We stress that our main result is the transition between the different regimes and not the minimum value of τ_m, which is specific to our model and has yet to be determined for 3d ferromagnets.

IV. CONCLUSION

In this paper we discussed the spin-dependent incoherent carrier dynamics due to electron-electron scattering in a ferromagnetic model system with spin-orbit coupling, which provide an extension of our earlier study of electron-phonon scattering in this system. We described a dynamical calculation using the spin-density matrix, spin-orbit coupling, and electron-electron scattering, which is nonlocal in k space, and compared the numerical results with a calculation using only occupation numbers and with a generalized relaxation-time ansatz. We found that the calculation using only occupation numbers failed to capture the demagnetization behavior for weak screening, i.e., strong scattering because the precessional dynamics around spin-orbit fields is neglected. The comparison with the generalized relaxation-time ansatz showed a very good agreement both for weak and strong Coulomb scattering, i.e., in situations where precessional dynamics of the off-diagonal part of the reduced spin-density matrix are clearly visible and also in cases where they are suppressed by scattering/dephasing. This suggests that the relaxation-time ansatz can capture essential properties of the incoherent spin-dependent dynamics using a k-local expression with a *single momentum relaxation time* τ. Such a simpler form should be useful in numerical calculations for more complicated problems in which scattering/dephasing due to the Coulomb interaction plays a role, such as transport and/or electronic dynamics due to coupling to magnons. In terms of the momentum relaxation time, we were able to fit the calculated demagnetization times using a sum of terms proportional to τ and τ^{-1}. The τ_m vs τ relationship is much simpler than the microscopic electron dynamics, and such a fit should be possible regardless of the details of the underlying band structure.

[1] I. Žutić, J. Fabian, and S. Das Sarma, Spintronics: Fundamentals and applications, Rev. Mod. Phys. **76**, 323 (2004).

[2] J. Fabian, A. Matos-Abiague, C. Ertler, and P. Stano, Semiconductor spintronics, Acta Phys. Slovaca **57**, 565 (2007).

[3] M. Wu and C. Ning, Dyakonov-Perel effect on spin dephasing in n-type GaAs, Phys. Status Solidi B **222**, 523 (2000).

[4] M. M. Glazov and E. L. Ivchenko, Dyakonov–Perel spin relaxation controlled by electron–electron scattering, J. Supercond. **16**, 735 (2003).

[5] Y. Yafet, g Factors and spin-lattice relaxation of conduction electrons, in *Solid State Physics* (Elsevier, New York, 1963), Vol. 14, pp. 1–98.

[6] B. Koopmans, G. Malinowski, F. Dalla Longa, D. Steiauf, M. Fähnle, T. Roth, M. Cinchetti, and M. Aeschlimann, Explaining the paradoxical diversity of ultrafast laser-induced demagnetization, Nat. Mater. **9**, 259 (2010).

[7] M. Krauß, T. Roth, S. Alebrand, D. Steil, M. Cinchetti, M. Aeschlimann, and H. C. Schneider, Ultrafast demagnetization

of ferromagnetic transition metals: The role of the Coulomb interaction, Phys. Rev. B **80**, 180407(R) (2009).

[8] B. Y. Mueller, A. Baral, S. Vollmar, M. Cinchetti, M. Aeschlimann, H. C. Schneider, and B. Rethfeld, Feedback Effect during Ultrafast Demagnetization Dynamics in Ferromagnets, Phys. Rev. Lett. **111**, 167204 (2013).

[9] J. K. Dewhurst, S. Shallcross, P. Elliott, S. Eisebitt, C. v. Korff Schmising, and S. Sharma, Angular momentum redistribution in laser-induced demagnetization, Phys. Rev. B **104**, 054438 (2021).

[10] P. Maldonado, T. Chase, A. H. Reid, X. Shen, R. K. Li, K. Carva, T. Payer, M. Horn von Hoegen, K. Sokolowski-Tinten, X. J. Wang, P. M. Oppeneer, and H. A. Dürr, Tracking the ultrafast nonequilibrium energy flow between electronic and lattice degrees of freedom in crystalline nickel, Phys. Rev. B **101**, 100302(R) (2020).

[11] S. R. Tauchert, M. Volkov, D. Ehberger, D. Kazenwadel, M. Evers, H. Lange, A. Donges, A. Book, W. Kreuzpaintner, U. Nowak, and P. Baum, Polarized phonons carry angular momentum in ultrafast demagnetization, Nature (London) **602**, 73 (2022).

[12] S. Eich, M. Plötzing, M. Rollinger, S. Emmerich, R. Adam, C. Chen, H. C. Kapteyn, M. M. Murnane, L. Plucinski, D. Steil, B. Stadtmüller, M. Cinchetti, M. Aeschlimann, C. M. Schneider, and S. Mathias, Band structure evolution during the ultrafast ferromagnetic-paramagnetic phase transition in cobalt, Sci. Adv. **3**, e1602094 (2017).

[13] M. Beens, R. A. Duine, and B. Koopmans, Modeling ultrafast demagnetization and spin transport: The interplay of spin-polarized electrons and thermal magnons, Phys. Rev. B **105**, 144420 (2022).

[14] S. Essert and H. C. Schneider, Electron-phonon scattering dynamics in ferromagnetic metals and their influence on ultrafast demagnetization processes, Phys. Rev. B **84**, 224405 (2011).

[15] K. Carva, M. Battiato, and P. M. Oppeneer, Ab Initio Investigation of the Elliott-Yafet Electron-Phonon Mechanism in Laser-Induced Ultrafast Demagnetization, Phys. Rev. Lett. **107**, 207201 (2011).

[16] K. Leckron, S. Vollmar, and H. C. Schneider, Ultrafast spin-lattice relaxation in ferromagnets including spin-orbit fields, Phys. Rev. B **96**, 140408(R) (2017).

[17] K. Leckron and H. C. Schneider, Ferromagnetic model system with spin-orbit coupling: Dynamical gap and effective spin-flip scattering, J. Magn. Magn. Mater. **471**, 482 (2019).

[18] D. A. Pesin and A. H. MacDonald, Quantum kinetic theory of current-induced torques in Rashba ferromagnets, Phys. Rev. B **86**, 014416 (2012).

[19] J. Ibañez-Azpiroz, A. Bergara, E. Y. Sherman, and A. Eiguren, Spin-flip transitions and departure from the Rashba model in the Au(111) surface, Phys. Rev. B **88**, 125404 (2013).

[20] P. Boross, B. Dóra, A. Kiss, and F. Simon, A unified theory of spin-relaxation due to spin-orbit coupling in metals and semiconductors, Sci. Rep. **3**, 3233 (2013).

[21] A. A. Burkov and L. Balents, Spin relaxation in a two-dimensional electron gas in a perpendicular magnetic field, Phys. Rev. B **69**, 245312 (2004).

[22] Y. Zhou, T. Yu, and M. W. Wu, Anomalous Dyakonov-Perel spin relaxation in semiconductor quantum wells under a strong magnetic field in the Voigt configuration, Phys. Rev. B **87**, 245304 (2013).

[23] A. Baral and H. C. Schneider, Magnetic switching dynamics due to ultrafast exchange scattering: A model study, Phys. Rev. B **91**, 100402(R) (2015).

[24] M. Wu, J. Jiang, and M. Weng, Spin dynamics in semiconductors, Phys. Rep. **493**, 61 (2010).

[25] K. Ishizaka, M. Bahramy, H. Murakawa, M. Sakano, T. Shimojima, T. Sonobe, K. Koizumi, S. Shin, H. Miyahara, A. Kimura *et al.*, Giant Rashba-type spin splitting in bulk bitei, Nat. Mater. **10**, 521 (2011).

[26] R. Binder and S. Koch, Nonequilibrium semiconductor dynamics, Prog. Quantum Electron. **19**, 307 (1995).

[27] H. Haug and A.-P. Jauho, *Quantum Kinetics in Transport and Optics of Semiconductors*, Solid-State Sciences No. 123 (Springer, Berlin, Heidelberg, 2008).

[28] M. Kira and S. W. Koch, *Semiconductor Quantum Optics* (Cambridge University Press, Cambridge, UK, New York, 2012).

[29] A. Baral, S. Vollmar, and H. C. Schneider, Magnetization dynamics and damping due to electron-phonon scattering in a ferrimagnetic exchange model, Phys. Rev. B **90**, 014427 (2014).

[30] S. Vollmar, Theoretische Beschreibung von Spin- und Magnetisierungsdynamik in Systemen mit Spin-Bahn-Kopplung und Austauschwechselwirkung, Ph.D. thesis, TU Kaiserslautern, 2018.

[31] H. Haug and S. W. Koch, *Quantum Theory of the Optical and Electronic Properties of Semiconductors*, 5th ed. (World Scientific, Singapore, 2009).

[32] D. Steiauf and M. Fähnle, Elliott-Yafet mechanism and the discussion of femtosecond magnetization dynamics, Phys. Rev. B **79**, 140401(R) (2009).

[33] C. Scholl, S. Vollmar, and H. C. Schneider, Off-resonant all-optical switching dynamics in a ferromagnetic model system, Phys. Rev. B **99**, 224421 (2019).

[34] P. H. Song and K. W. Kim, Spin relaxation of conduction electrons in bulk III-V semiconductors, Phys. Rev. B **66**, 035207 (2002).

[35] Z. G. Yu, S. Krishnamurthy, M. van Schilfgaarde, and N. Newman, Spin relaxation of electrons and holes in zinc-blende semiconductors, Phys. Rev. B **71**, 245312 (2005).

[36] S. Vollmar, D. J. Hilton, and H. C. Schneider, Generalized Elliott-Yafet spin-relaxation time for arbitrary spin mixing, Phys. Rev. B **96**, 075203 (2017).

[37] J. Dormand and P. Prince, A family of embedded Runge-Kutta formulae, J. Comput. Appl. Math. **6**, 19 (1980).